IIETA International Information and Engineering Technology Association
Advancing the World of Information and Engineering

Mathematical Modelling of Engineering Problems
Vol. 6, No. 4, December, 2019, pp. 502-510
Journal homepage: http://iieta.org/journals/mmep

Multiple Slips Effects on MHD Thermo-Solutal Flow in Porous Media Saturated by Nanofluid

Fazle Mabood[1*], Halima Usman[2]

[1] Department of Information Technology, Fanshawe College London, ON, Canada
[2] Department of Mathematics, Usmanu Danfodiyo University, Sokoto, Nigeria

Corresponding Author Email: fmabood@fanshawec.ca

https://doi.org/10.18280/mmep.060404

Received: 3 September 2019
Accepted: 17 October 2019

Keywords:
HAM, heat transfer, mass transfer, MHD, multiple slip, nanofluid, porous media

ABSTRACT

In this article, the effect of multiple slips on the boundary layer flow of MHD nanofluid with heat and mass transfer past a vertical plate embedded in a Darcy porous media is investigated. Instead of using conventional no slip boundary conditions, we use velocity, thermal and mass slip boundary conditions so as to obtain more realistic results compared to some earlier studies, for certain physical situations. Our nanofluid model incorporates Brownian motion and thermophoresis effects. The governing boundary layer equations are converted to nonlinear ordinary differential equations using similarity transformations and the resulting equations are solved using the homotopy analysis method (HAM). The effects of the governing parameters on velocity, temperature, nanoparticles concentration field as well as on the skin friction coefficient, reduced Nusselt and Sherwood numbers are made appropriately via graphs and charts and explained the consequences with proper reasoning

1. INTRODUCTION

Convection is of fundamental interest in numerous engineering, industrial, and environmental applications such as cooling of electronic devices, air-conditioning systems, atmospheric flows, and security of energy systems and in designs related to thermal insulation. Fluid flow and heat transfer through porous media has been discussed in detail and reviewed by Nield and Beja [1], Vafai [2] as well as Adler and Brenner [3]. A closed form solution of the Brinkman-Forchheimer equation due the forced convection in a fluid saturated porous medium with isothermal and isoflux boundaries was obtained by Nield et al. [4] valid for all values of the Darcy number. Other studies include that of Ahmad and Pop [5] who investigated the mixed convection boundary layer flow over a vertical flat plate embedded in a porous medium saturated with a nanofluid, Kuznetsov and Nield [6] have studied the Brinkman model and provided the thermal instability in porous medium layer filled with nanofluid. Further, Khan and Pop [7] extended the study and idea of Kuznetsov and Nield [8] for the case of stretching surface in nanofluid. However, in the above studies [5-7] the authors have considered the no-slip boundary conditions and the transformed equations are solved numerically. Much of the literature on boundary layer flow over various geometries such as horizontal/vertical plate, cone, rotating disk deals with no-slip boundary conditions at the solid fluid interface and relatively less attention has thus for been given to slip boundary conditions. For flows around micro-scale/nano-scale devices, we have to include slip boundary conditions [9]. Various other researchers have investigated slip flow for different situations [10-18].

In general transport problems are governed by systems of nonlinear partial differential equation (PDE) subject to relevant initial and boundary conditions. Closed form solutions are often difficult to obtain. The system of PDEs is usually converted into a corresponding system of ordinary differential equations (ODEs) using similarity analysis techniques. The ODEs which are usually nonlinear can be solved by various semi-analytical methods, numerical methods but numerical methods are often computationally expensive. Several semi-analytical methods have been suggested to solve the associated nonlinear ODEs. These methods include the modified decomposition method [19] and the homotopy analysis method [20-23]. The aim of our present paper is to obtain an accurate analytical solution, via the homotopy analysis method for a velocity/thermal/solutal slip in hydromagnetic nanofluid flow involving in porous media. In the sense of comparison with other approximate analytical method, HAM yields a family of solution expressions in the auxiliary parameter $\hbar$. The analytical solutions obtained, albeit approximate, allows for a deeper understanding and overview of the understanding physical phenomena.

2. GOVERNING EQUATIONS

A two-dimensional steady flow with a coordinate system such that the $\bar{x}$-axis is aligned vertically and the $\bar{y}$-axis is normal to it is considered. A transverse magnetic field B_0 is assumed to act parallel to the $\bar{y}$-axis. The magnetic Reynolds number is assumed small so that the induced magnetic field is negligible. The electric field related to the polarization of charges and Hall effects is neglected. The four relevant equations are the equations of conservation of mass, momentum, thermal energy, and the nanoparticles volume fraction which can be written in dimensional forms, extending the formulations of Buongiorno [24] as:

$$\frac{\partial \bar{u}}{\partial \bar{x}} + \frac{\partial \bar{v}}{\partial \bar{y}} = 0 \tag{1}$$

$$\rho_f \left(\bar{u} \frac{\partial \bar{u}}{\partial \bar{x}} + \bar{v} \frac{\partial \bar{u}}{\partial \bar{y}} \right) = \mu \frac{\partial^2 \bar{u}}{\partial \bar{y}^2} - \frac{\mu}{k} \bar{u} - \sigma B_0^2 \bar{u} \tag{2}$$

$$\bar{u} \frac{\partial T}{\partial \bar{x}} + \bar{v} \frac{\partial T}{\partial \bar{y}} = \alpha \frac{\partial^2 T}{\partial \bar{y}^2} + \tau \left\{ D_B \frac{\partial C}{\partial \bar{y}} \frac{\partial T}{\partial \bar{y}} + \left(\frac{D_T}{T_\infty} \right) \left(\frac{\partial T}{\partial \bar{y}} \right)^2 \right\} \tag{3}$$

$$\bar{u} \frac{\partial C}{\partial \bar{x}} + \bar{v} \frac{\partial C}{\partial \bar{y}} = D_B \frac{\partial^2 C}{\partial \bar{y}^2} + \left(\frac{D_T}{T_\infty} \right) \frac{\partial^2 T}{\partial \bar{y}^2} \tag{4}$$

The appropriate boundary conditions are [9]:

$$\begin{aligned} &\bar{u} = u_w + \bar{u}_{\text{slip}},\ \bar{v} = v_w,\ T = T_w + T_{slip}, \\ &C = C_w + C_{slip} \quad \text{at} \quad \bar{y} = 0, \\ &\bar{u} \to 0,\ T \to T_\infty,\ C \to C_\infty \quad \text{as} \quad \bar{y} \to \infty \end{aligned} \tag{5}$$

Here $\alpha = \frac{k}{(\rho\, c)_f}$: thermal diffusivity of the fluid, $\tau = \frac{(\rho\, c)_p}{(\rho\, c)_f}$: ratio of heat capacity of the nanoparticle and fluid, K_p: permeability of the medium, ($\bar{u}, \bar{v}$): velocity components along $\bar{x}$ and $\bar{y}$ axes, $\bar{u}_e = \frac{U_r \bar{x}}{L}$: velocity of the plate, L : characteristic length of the plate, $\bar{u}_{\text{slip}} = N_1 \nu \frac{\partial \bar{u}}{\partial \bar{y}}$: linear slip velocity, N_1: velocity slip factor, $T_{\text{slip}} = D_1 \frac{\partial T}{\partial \bar{y}}$: thermal slip, D_1: thermal slip factor, $C_{\text{slip}} = E_1 \frac{\partial C}{\partial \bar{y}}$: mass slip, E_1: mass slip factor, ρ_f density of the base fluid, μ dynamic viscosity of the base fluid, ρ_p density of the nanoparticles, $(\rho C_P)_f$: heat effective heat capacity of the fluid, $(\rho C_P)_P$: effective heat capacity of the nanoparticle material, D_B Brownian diffusion coefficient, D_T: thermophoretic diffusion.

We define the following dimensionless transformation variables:

$$\begin{aligned} &\eta = \frac{\bar{y}}{\sqrt{K_p}},\ \psi = U_r \frac{\bar{x}}{L} \sqrt{K_p}\, f(\eta), \\ &\theta(\eta) = \frac{T - T_\infty}{T_w - T_\infty},\ \phi(\eta) = \frac{C - C_\infty}{C_w - C_\infty} \end{aligned} \tag{6}$$

3. SIMILARITY EQUATIONS

Substitution of (6) into Eqns. (1)-(5) generate the following similarity equations:

$$f''' - f' + \text{Re} Da \left(f f'' - f'^2 - M^2 f' \right) = 0 \tag{7}$$

$$\theta'' + Da \,\text{Pr}\, Ref\, \theta' + \text{Pr} \left[Nb \theta' \phi' + Nt \theta'^2 \right] = 0 \tag{8}$$

$$\phi'' + Da Le \,\text{Re}\, f \phi' + \frac{Nt}{Nb} \theta'' = 0 \tag{9}$$

The relevant boundary conditions are:

$$\begin{aligned} &f(0) = 0,\ f'(0) = 1 + a\ f''(0), \theta(0) = 1 + b\, \theta'(0), \\ &\phi(0) = 1 + c\ \phi'(0),\ f'(\infty) = 0, \theta(\infty) = \phi(\infty) = 0 \end{aligned} \tag{10}$$

where, primes denote differentiation with respect to η. The thermo-physical dimensionless parameters arising in Eqns. (7)-(10) are defined as follows: $\text{Re} = U_r L / \nu$ is the Reynolds number, $Da = K_p / L^2$ is the Darcy number, $M = \sigma B_0^2 L / U_r \rho$ is the magnetic field parameter, $\text{Pr} = \nu / \alpha$ is the Prandtl number, $Nt = \tau D_T \left(T_w - T_\infty \right) / \nu T_\infty$ is the thermophoresis parameter, $Nb = \tau D_B \left(C_w - C_\infty \right) / \nu$ is the Brownian motion parameter, $Le = \nu / D_B$ is the Lewis number, $a = N_1 \nu / \sqrt{K_P}$ is the hydrodynamic (momentum) slip parameter, $b = D_1 / \sqrt{K_P}$ is the thermal slip parameter, $c = E_1 / \sqrt{K_P}$ is the mass slip parameter, and $f_w = v_w L / U_r \sqrt{K_P}$ is the suction/injection parameter. Note that all the dimensionless parameters are free from axial distance x and confirm the true similarity of the problem.

The quantities of physical interest in our study are the local friction factor, $C_{f\bar{x}}$, the local Nusselt number, $Nu_{\bar{x}}$, the local Sherwood number $Sh_{\bar{x}}$. Physically, C_{fx} represents the wall shear stress, $Nu_{\bar{x}}$, defines the heat transfer rates and $Sh_{\bar{x}}$ defines the mass transfer rates.

$$C_{fx}\, \text{Re}_x^{-1}\, Da_x^{0.5} = 2 f''(0) \tag{11}$$

$$Nu_{\bar{x}}\, Da_{\bar{x}}^{0.5} = -\theta'(0),\ Sh_{\bar{x}}\, Da_{\bar{x}}^{0.5} = -\phi'(0) \tag{12}$$

where, $Da_{\bar{x}} = K_p / \bar{x}^2$ is the local Darcy number for Darcian porous media and $\text{Re}_{\bar{x}} = \bar{u}_w \bar{x} / \nu$ is the local Reynolds number.

Note that for purely hydromagnetic boundary layer ($M = 0$), no slip boundary conditions ($a = b = c = 0$), the problem reduces to the problem which has been recently investigated by Dayyan et al. [14] when $Da = 1$, $Nt = 0, Nb \to 0$ in our model and $n = 0$ in their model. This provides a validation of our model.

4. HOMOTOPY ANALYSIS METHOD

The HAM procedure described in this section is based on the work of [20-23]. For HAM solution of the governing Eqns. (7), (8) and (9) subject to the boundary conditions (10), the initial approximations for velocity $f(\eta)$, temperature $\theta(\eta)$ and concentration $\phi(\eta)$ are chosen as follows:

$$f_0(\eta) = \frac{e^{-\eta} - 1}{1 + a},\ \theta_0(\eta) = \frac{e^{-\eta}}{1 + b},\ \phi_0(\eta) = \frac{e^{-\eta}}{1 + c} \tag{13}$$

the auxiliary linear operators are:

$$L_f = \frac{d^3 f}{d\eta^3} - \frac{df}{d\eta},\ L_\theta = \frac{d^2\theta}{d\eta^2} - \theta,\ L_\phi = \frac{d^2\phi}{d\eta^2} - \phi \tag{14}$$

with properties

$$L_f\left(C_1 + C_2 e^{\eta} + C_3 e^{-\eta}\right) = 0$$
$$L_\theta\left(C_4 e^{\eta} + C_5 e^{-\eta}\right) = 0\ L_\phi\left(C_6 e^{\eta} + C_7 e^{-\eta}\right) = 0 \tag{15}$$

where, $C_i\,(i = 1-7)$ are constants.

Next, construct the following homotopy for the Eqns. (7), (8) and (9),

$$(1-p)\ L_f\left[\hat{f}(\eta,p) - f_0(\eta)\right] = p\hbar_f\ N_f\left[\hat{f}(\eta,p)\right] \tag{16}$$

$$(1-p)\ L_\theta\left[\hat{\theta}(\eta,p) - \theta_0(\eta)\right] = p\hbar_\theta\ N_\theta\left[\hat{\theta}(\eta,p), \hat{f}(\eta,p)\right] \tag{17}$$

$$(1-p)\ L_\phi\left[\hat{\phi}(\eta,p) - \phi_0(\eta)\right] = p\hbar_\phi\ N_\phi\left[\hat{\phi}(\eta,p), \hat{f}(\eta,p)\right] \tag{18}$$

subject to the boundary conditions

$$\hat{f}(0,p) = 0,\quad \hat{f}'(0,p) = 1 + a\hat{f}''(0,p),\quad \hat{f}'(\infty,p) = 0 \tag{19}$$

$$\hat{\theta}(0,p) = 1 + b\hat{\theta}'(0,p),\quad \hat{\theta}(\infty,p) = 0 \tag{20}$$

$$\hat{\phi}(0,p) = 1 + c\hat{\phi}'(0,p),\quad \hat{\phi}(\infty,p) = 0 \tag{21}$$

where, N_f, N_θ and N_ϕ are non-linear operators, which are defined as:

$$N_f\left[\hat{f}(\eta,p)\right] = \frac{\partial^3 \hat{f}(\eta,p)}{\partial\eta^3} - \frac{\partial \hat{f}(\eta,p)}{\partial\eta} + Da\,\mathrm{Re}\left(\hat{f}(\eta,p)\frac{\partial^2 \hat{f}(\eta,p)}{\partial\eta^2} - \left(\frac{\partial \hat{f}(\eta,p)}{\partial\eta}\right)^2 - M^2\frac{\partial \hat{f}(\eta,p)}{\partial\eta}\right) \tag{22}$$

$$N_\theta\left[\hat{\theta}(\eta,p), \hat{f}(\eta,p)\right] = \left\{\frac{\partial^2 \hat{\theta}(\eta,p)}{\partial\eta^2} + Da\,\mathrm{Pr}\,Re\hat{f}(\eta,p)\frac{\partial\hat{\theta}(\eta,p)}{\partial\eta} + \mathrm{Pr}\left(N_b\frac{\partial\hat{f}(\eta,p)}{\partial\eta}\hat{\theta}(\eta,p) + N_t\left(\frac{\partial\hat{\theta}(\eta,p)}{\partial\eta}\right)^2\right)\right. \tag{23}$$

$$N_\phi\left[\hat{\phi}(\eta,p), \hat{f}(\eta,p)\right] = \frac{\partial^2 \hat{\phi}(\eta,p)}{\partial\eta^2} + DaLe\,\mathrm{Re}\,\hat{f}(\eta,p)\frac{\partial\hat{\phi}(\eta,p)}{\partial\eta} + \frac{N_t}{N_b}\frac{\partial^2\hat{\theta}(\eta,p)}{\partial\eta^2}. \tag{24}$$

and p is the embedding parameter.

When p increases from 0 to 1, $f(\eta,p)$, $\theta(\eta,p)$ and $\phi(\eta,p)$ vary from $f_0(\eta,p)$, $\theta_0(\eta,p)$ and $\phi_0(\eta,p)$ to $f(\eta,p)$, $\theta(\eta,p)$ and $\phi(\eta,p)$ respectively. Using Taylor's series, we can write

$$\hat{f}(p,\eta) = f_0(\eta) + \sum_{m=1}^{+\infty} f_m(\eta)\,p^m,\quad f_m(\eta) = \frac{1}{m!}\frac{\partial^m f(\eta,p)}{\partial\eta^m}\bigg|_{p=0} \tag{25}$$

$$\hat{\theta}(p,\eta) = \theta_0(\eta) + \sum_{m=1}^{+\infty} \theta_m(\eta)\,p^m,\quad \theta_m(\eta) = \frac{1}{m!}\frac{\partial^m \theta(\eta,p)}{\partial\eta^m}\bigg|_{p=0} \tag{26}$$

$$\hat{\phi}(p,\eta) = \phi_0(\eta) + \sum_{m=1}^{+\infty} \phi_m(\eta)\,p^m,\quad \phi_m(\eta) = \frac{1}{m!}\frac{\partial^m \phi(\eta,p)}{\partial\eta^m}\bigg|_{p=0}. \tag{27}$$

The convergence of the series (25), (26) and (27) is dependent as auxiliary parameters $\hbar_f$, $\hbar_\theta$ and $\hbar_\phi$. Let us assume that the auxiliary parameters are chosen such that series (25), (26) and (27) are convergent at $p = 1$. From (25), (26) and (27),

$$f(\eta) = f_0(\eta) + \sum_{m=1}^{+\infty} f_m(\eta),\quad \theta(\eta) = \theta_0(\eta) + \sum_{m=1}^{+\infty} \theta_m(\eta),\quad \phi(\eta) = \phi_0(\eta) + \sum_{m=1}^{+\infty} \phi_m(\eta) \tag{28}$$

The *m*th-order deformation equations can be obtained by differentiating Eqns. (16), (17) and (18) *m* times with respect to *p*, and subsequently dividing by *m*! at *p* = 0. We then have

$$L_f\left[f_m(\eta) - \chi_m f_{m-1}(\eta)\right] = \hbar_f\,\mathrm{R}_m^f(\eta) \tag{29}$$

$$L_\theta\left[\theta_m(\eta) - \chi_m\theta_{m-1}(\eta)\right] = \hbar_\theta\mathrm{R}_m^\theta(\eta) \tag{30}$$

$$L_\phi\left[\phi_m(\eta) - \chi_m\phi_{m-1}(\eta)\right] = \hbar_\phi\mathrm{R}_m^\phi(\eta) \tag{31}$$

subject to boundary conditions

$$\begin{cases} f_m(0)=0,\ f_m'(0)=af_m''(0), \\ \theta_m(0)=b\theta_m'(0),\phi_m(0)=c\phi_m'(0), \\ f_m'(\infty)=0,\theta_m(\infty)=0,\phi_m(\infty)=0 \end{cases} \tag{32}$$

Here the remainder terms are as follows

$$\mathrm{R}_m^f(\eta)=f_{m-1}'''(\eta)-f_{m-1-k}'+ Da\,\mathrm{Re}\left(\sum_{k=0}^{m-1}f_k f_{m-1-k}''-\sum_{k=0}^{m-1}f_k' f_{m-1-k}'-Mf_{m-1-k}'\right) \tag{33}$$

$$\mathrm{R}_m^\theta(\eta)=\theta_{m-1}''(\eta)+Da\,\mathrm{Pr}\,\mathrm{Re}\sum_{k=0}^{m-1}f_k\theta_{m-1-k}'+ \mathrm{Pr}\left(N_b\sum_{k=0}^{m-1}\theta_k'\phi_{m-1-k}'+N_t\sum_{k=0}^{m-1}\theta_k'\theta_{m-1-k}'\right) \tag{34}$$

$$\mathrm{R}_m^\phi(\eta)=\phi_{m-1}''(\eta)+ DaLe\,\mathrm{Re}\sum_{k=0}^{m-1}f_k\phi_{m-1-k}'+\frac{N_t}{N_b}\theta_{m-1}''(\eta) \tag{35}$$

$$\chi_m=\begin{cases}0, & m\le 1,\\ 1, & m>1.\end{cases} \tag{36}$$

The general solution of Eq. (28) is:

$$f_m(\eta)=f_m^*(\eta)+C_1+C_2\exp(\eta)+C_3\exp(-\eta) \tag{37}$$

$$\theta_m(\eta)=\theta_m^*(\eta)+C_4\exp(\eta)+C_5\exp(-\eta) \tag{38}$$

$$\phi_m(\eta)=\phi_m^*(\eta)+C_6\exp(\eta)+C_7\exp(-\eta) \tag{39}$$

where, $f_m^*(\eta)$, $\theta_m^*(\eta)$ and $\phi_m^*(\eta)$ denote the special solutions for Eqs. (29), (30) and (31) and the constants are determined by employing the boundary condition Eq. (28). The residual errors for the HAM 15th order approximation solution are defined as:

$$\mathrm{Res}_f=\frac{d^3f}{d\eta^3}-\frac{df}{d\eta}+ \mathrm{Re}\,\mathrm{Da}\left(f\frac{d^2f}{d\eta^2}-\left(\frac{df}{d\eta}\right)^2-M^2\frac{df}{d\eta}\right) \tag{40}$$

$$\mathrm{Res}_\theta=\frac{d^2\theta}{d\eta^2}+Da\,\mathrm{Pr}\,\mathrm{Re}\left(f\frac{d\theta}{d\eta}\right)+ \mathrm{Pr}\left(Nb\frac{d\theta}{d\eta}\frac{d\phi}{d\eta}+Nt\left(\frac{d\theta}{d\eta}\right)^2\right) \tag{41}$$

$$\mathrm{Res}_\phi=\frac{d^2\phi}{d\eta^2}+DaLe\,\mathrm{Re}\left(f\frac{d\phi}{d\eta}\right)+\frac{Nt}{Nb}\frac{d^2\theta}{d\eta^2} \tag{42}$$

5. CONVERGENCE OF THE HAM SOLUTION

Eqns. (37), (38) and (39) yield an analytical solution of the problem in the form of series. The convergence depends on the auxiliary parameters $\hbar_f,\hbar_\theta,\hbar_\phi$ [20]. These parameters, as was pointed out by previous researchers can be used to adjust and control the convergence region and convergence rate. So that appropriate values for these auxiliary parameters, the so called $\hbar_f$, $\hbar_\theta$ and $\hbar_\phi$ curves are displayed at 15th order approximations as shown in Figure 1. Figure 1 also shows that the dimensionless velocity converges when $-1.8<\hbar_f<-0.25$, the dimensionless temperature converges when $-1.6<\hbar_\theta<-0.5$, and the dimensionless concentration converges for $-1.5<\hbar_\phi<-0.2$. Figure 1 shows the $\hbar$ curves for the dimensionless velocity, temperature and concentration. Convergence of the series solution up to 40th order of approximations is presented in Table 1. For validation of the obtained homotopy simulation in the present article, we compared the numerical results of [14, 19] in Table 2 and Table 3 and an excellent agreement is observed. The variation of skin friction coefficient, Nusselt and Sherwood numbers for various values of parameters is presented in Table 4.

Table 1. Convergence of HAM solutions for different order of approximations at $M=\mathrm{Re}=1,\ \mathrm{Pr}=6.8,\ Le=10,\ Da=0.3,\ Nb=Nt=0.2,\ a=b=c=0.4,\hbar_f=-0.8,\hbar_\theta=\hbar_\phi=-1$

Order of approximation	$-f''(0)$	$-\theta'(0)$	$-\phi'(0)$
1	0.81924	0.25267	0.38630
5	0.82228	0.21782	0.58916
15	0.82228	0.21223	0.58267
23	0.82228	0.21200	0.58272
30	0.82228	0.21200	0.58272
40	0.82228	0.21200	0.58272
[Numerical]	[0.82228]	[0.21200]	[0.58272]

Table 2. Comparison of $-f''(0)$ for various values of Re at $Da=1,\ a=M=0$

M	Re	Dayan el al. [14]	Hayat et al. [19]	Present results
0	1	1.4242	1.4142	1.4142
	1.5	1.5811	-	1.5810
	2	1.7320	-	1.7321
	5	2.4494	-	2.4495
2	1	-	2.4494	2.4494
3		-	3.3166	3.3166
7		-	7.1414	7.1414
$\sqrt{99}$		-	10.0498	10.0498

Table 3. Comparison of heat transfer rate for various values of Re at $\mathrm{Pr}=Da=M=1,\ a=b=c=N_b=N_t=0$

Re	Dayan et al. [14]	Present results
1	0.5033	0.5029
1.5	0.6422	0.6419
2	0.7592	0.7594
5	1.2576	1.2576

Table 4. Results of skin friction coefficient, Nusselt and Sherwood numbers for various values of parameters at $\Pr = 6.8$, $\mathrm{Re} = 5$, $M = 0$, $Le = 5$, $Nb = Nt = 0.1$

A	b	c	Da	$-f''(0)$	$-\theta'(0)$	$-\phi'(0)$
0	0	0	0	1.00000	0.04696	0.15304
0.5				0.66666	0.04696	0.15304
1				0.50000	0.04696	0.15304
0.4	0	0	0	0.71429	0.04696	0.15304
	0.5			0.71429	0.04631	0.15137
	1			0.71429	0.04566	0.14976
0.5	0.5	0	0	0.66667	0.04631	0.15137
		0.5		0.66667	0.04768	0.14280
		1		0.66667	0.04892	0.13512
0.2	0.2	0.2	0	0.83333	0.04728	0.14882
			0.7	1.36746	1.41331	1.59144
			1	1.49052	1.60736	1.31367

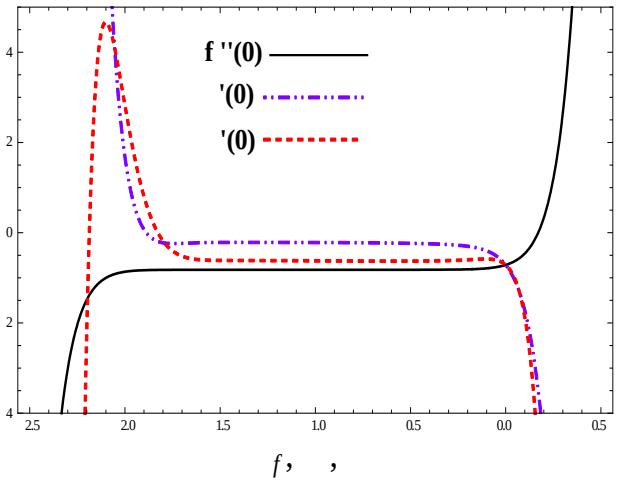

Figure 1. The *h*-curves of $f''(0)$, $\theta'(0)$ and $\phi'(0)$ are obtained by the 15th-order approximation at $M = \mathrm{Re} = 1, \Pr = 6.8, Le = 10, Da = 0.3,$ $Nb = Nt = 0.2, a = b = c = 0.4$

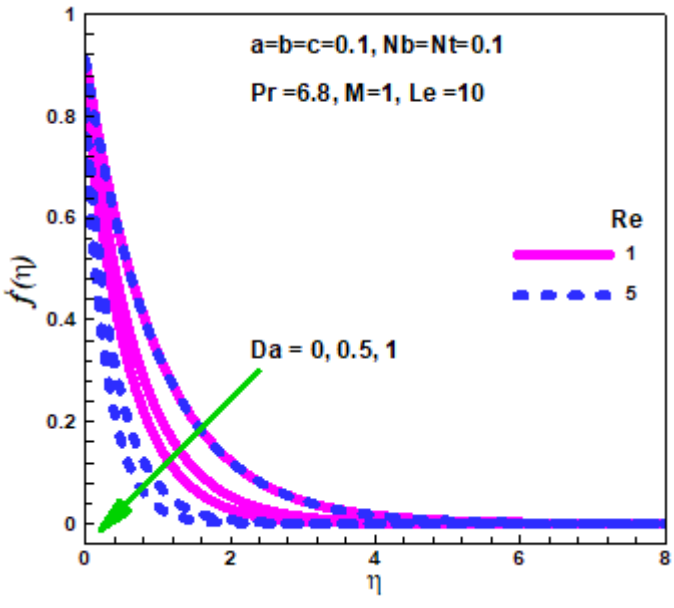

Figure 2. Effects of Da and Re on dimensionless velocity

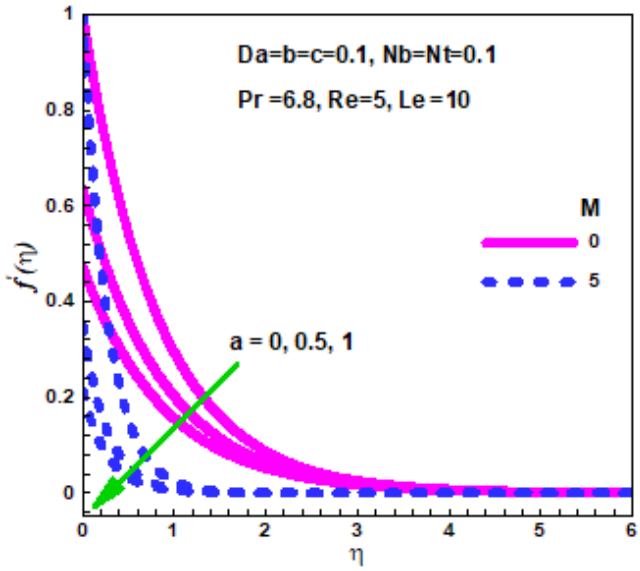

Figure 3. Effects of *a* and *M* on dimensionless velocity

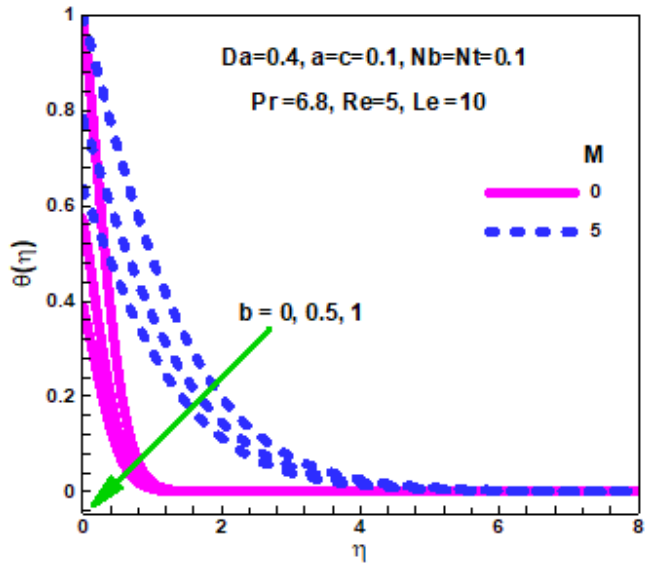

Figure 4. Effects of *b and M* on dimensionless temperature

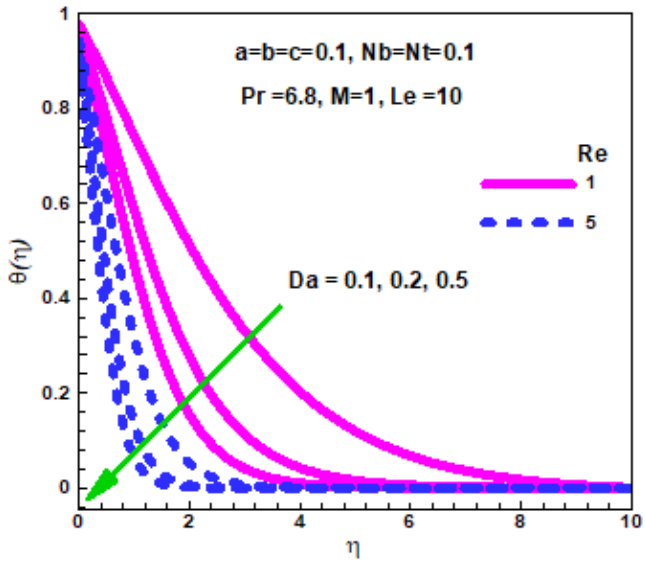

Figure 5. Effects of *Da* and *Re* on dimensionless temperature

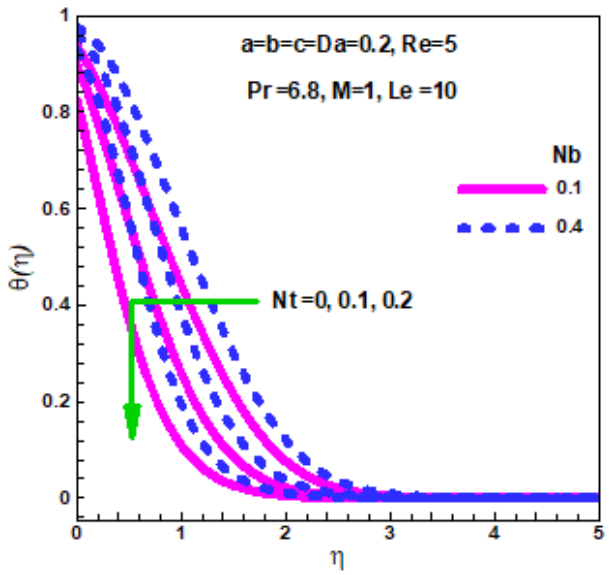

Figure 6. Effects of *b*, *M* on dimensionless temperature

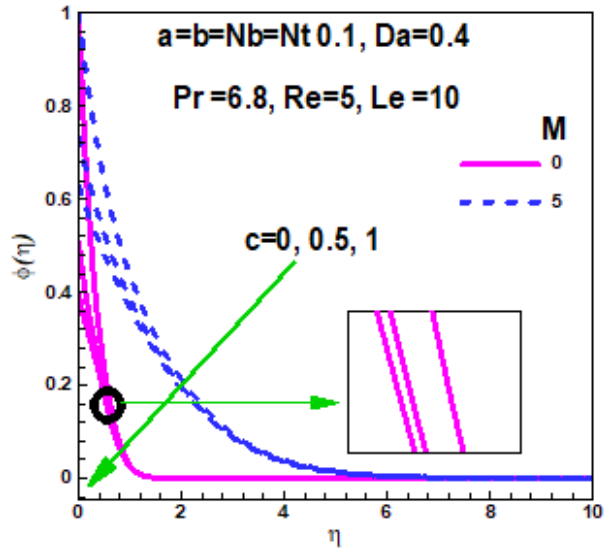

Figure 7. Effects of *c* and *M* dimensionless concentration

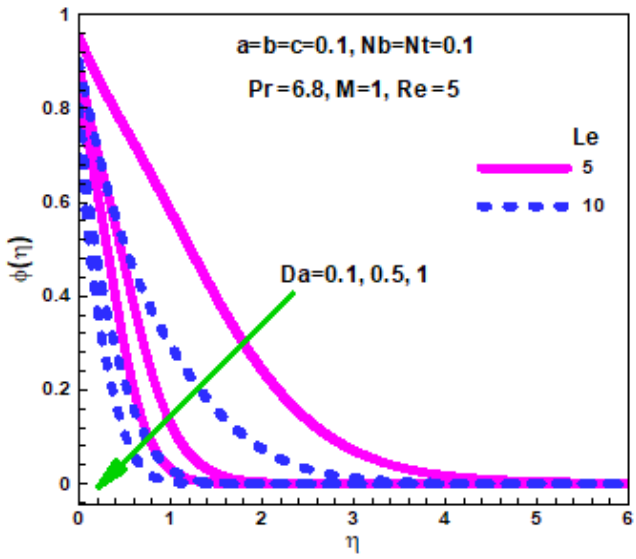

Figure 8. Effects of Da and *Le* on dimensionless concentration

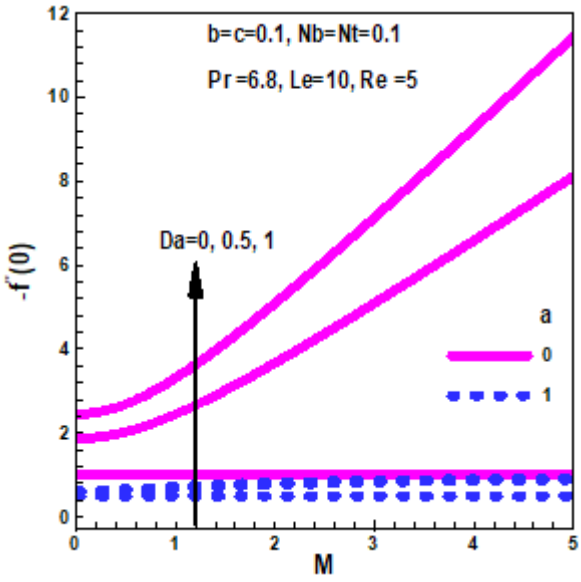

Figure 9. Variation of skin friction coefficient against *M*, *Da* and *a*

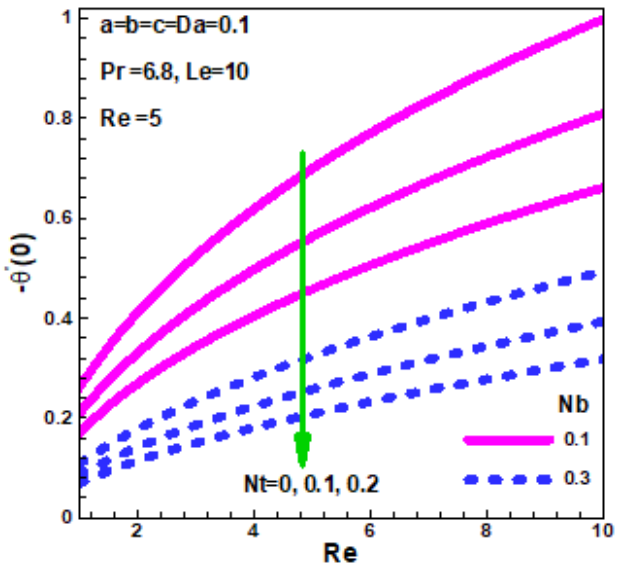

Figure 10. Variation of heat transfer rate against *Re*, *Nb* and *Nt*

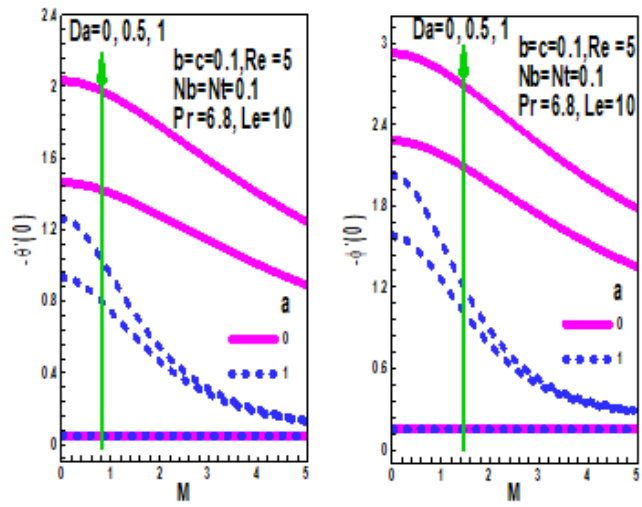

Figure 11. Variation of heat and mass transfer rates against *M*, *a* and *Da*

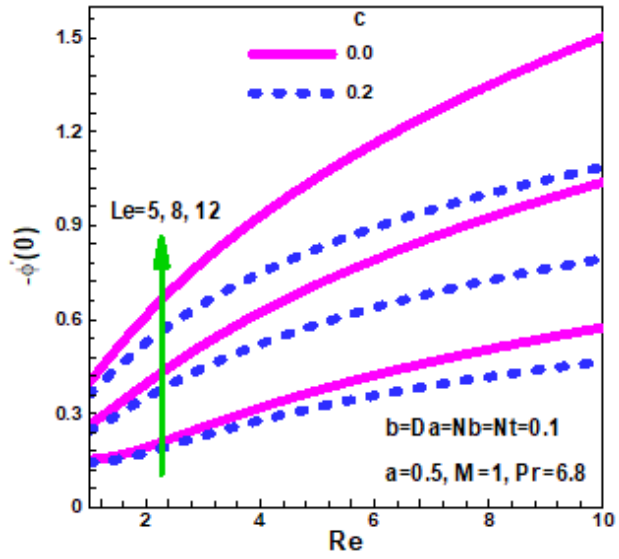

Figure 12. Variation of mass transfer rate against *Re*, *Le* and *c*

6. RESULTS AND DISCUSSION

Figure 2 shows the variation of the dimensionless velocity inside the boundary layer with the Darcy number and the Reynolds number. The dimensionless velocity is decreased as both the Darcy number the Reynold numbers increase. A similar trend of velocity was also noticed by Dayyan et al. [14]. The magnetic field and the velocity slip effects on the dimensionless velocity are shown in Figure 3. It is found that velocity slip reduces the velocity inside the boundary layer for both in the absence and presence of magnetic field. As usual, magnetic field dampen the velocity for both the conventional no slip ($a = 0$) and slip boundary condition.

The magnetic field and the thermal slip effect on the dimensionless temperature are displayed in Figure 4. Thermal slip reduces the temperature within the thermal boundary layer for both in the absence and presence of magnetic field. Magnetic field intensify the temperature for both the isothermal plate ($b = 0$) and non-isothermal plate ($b \neq 0$) . Figure 5 demonstrates that with an increase in both the Darcy number and Reynolds number, the concentration is suppressed within the solutal boundary layer. The effect of nanofluid parameters on dimensionless temperature is shown in Figure 6. It is found that temperature is reduced with the thermophoresis parameter and increased with the Brownian motion parameter. The magnetic field and the solutal slip effect on the dimensionless concentration are shown in Figure 7. It is found that concentration is reduced as the solutal slip parameter increases for both in the absence and presence of magnetic field. As usual, magnetic field enhances the concentration for both the isosolutal plate ($c=0$) and mass slip boundary condition. Figure 8 demonstrates that increasing Darcy number reduces the concentration. Lewis number is also reduces the dimensionless concentration. Asymptotic convergence of all profiles in Figures 2-8 is noticed. We now focus on the effect of the controlling parameters on the physical quantities. Figure 9 demonstrates the effects of the Darcy number, velocity slip parameter and the magnetic field parameter on the friction factor. It is noticed that friction increases as the Darcy number and the magnetic field parameter increase for both slip flow and no slip flow. Note that the effect of the Darcy number and the magnetic field are prominent for no slip flow.

Figure 10 demonstrates the effects of the Darcy number, velocity slip parameter and the magnetic field parameter on the heat and mass transfer rate. It is noticed that heat and mass transfer increase as the Darcy number increases whilst they decrease as the magnetic field parameter and velocity slip parameter increase. The effects of the nanofluid parameters on the heat transfer rates are illustrated in Figure 11. It is found that both the Brownian motion and thermophoresis parameter decrease whilst the Reynolds number increases the heat transfer rates. Finally, Fig. 12 illustrated the influence of the Reynolds number, Lewis number and the mass velocity on the mass transfer rates. It is found that mass transfer rates increases as the Reynolds number and Lewis number increases whilst it decreases with the increasing of mass slip parameter.

7. CONCLUSIONS

In this paper, we developed a mathematical model for steady-state two-dimensional viscous incompressible magnetohydrodynamic slip flow of nanofluid past a vertical plate in a Darcian porous medium. The governing equations were transformed into a system of ODE using similarity transformation. The homotopy analysis method, which is a semi-analytical method, was used to solve this system. The main findings are:

- Increasing Darcy number and magnetic field parameters lead to increase the friction.
- The heat and mass transfer rates increase as the Darcy number increases whilst they decrease as the magnetic field parameter and velocity slip parameter increase.
- The Brownian motion and thermophoresis parameter decrease whilst the Reynolds number increases the heat transfer rates.
- The mass transfer rates increases as the Reynolds number and Lewis number increase whilst it decreases with the increasing of mass slip parameter. It is presumed that, with the help of the present model, the physics of the flow along the vertical channel can be utilized as the basis for many engineering and scientific applications. The findings of the present problem are also of great interest in engineering, industrial, and environmental applications such as in cooling of electronic devices, air-conditioning systems, e.t.c.

REFERENCES

[1] Nield, D.A., Bejan, A. (2013). Convection in Porous Media. Springer, New York.

[2] Vafai, K. (2010). Porous Media: Applications in Biological Systems and Biotechnology. CRC Press, New York.

[3] Adler, P.M., Brenner, H. (1988). Multiphase flow in porous media. Annual Review of Fluid Mechanics, 20: 35-59.

[4] Nield, D.A., Junqueira, S.L.M., Lage, J.L. (1996). Forced convection in a fluid saturated porous medium channel with isothermal or isoflux boundaries. Journal of Fluid

Mechanics, 322: 201-214. https://doi.org/10.1017/S0022112096002765
[5] Ahmad, S., Pop, I. (2010). Mixed convection boundary layer flow from a vertical flat plate embedded in a porous medium filled with nanofluids. International Communication in Heat and Mass Transfer, 37(8): 987-991. https://doi.org/10.1016/j.icheatmasstransfer.2010.06.004
[6] Kuznetsov, A.V., Nield, D.A. (2010). Thermal instability in a porous medium layer saturated by a nanofluid: Brinkman model. Trans Porous Media, 81(3): 409-422. https://doi.org/10.1007/s11242-009-9413-2
[7] Khan, W.A., Pop, I. (2012). Boundary layer flow past a stretching surface in a porous medium saturated by a nanofluid: Brinkman-Forchheimer Model. PLoS ONE 7(10): e47031. https://doi.org/10.1371/journal.pone.0047031
[8] Kuznetsov, A.V., Nield, D.A. (2014). Natural convective boundary-layer flow of a nanofluid past a vertical plate. International Journal of Thermal Sciences, 49(2): 243-247. https://doi.org/10.1016/j.ijthermalsci.2009.07.015
[9] Karniadakis, G., Beskok, A., Aluru, N. (2005). Microflows and nanoflows fundamentals and simulation in microflows and nanoflows fundamentals and simulation. Springer, New York.
[10] Wang, C.Y. (2006). Stagnation slip flow and heat transfer on a moving plate. Chemical Engineering Science, 61(23): 7668-7672. https://doi.org/10.1016/j.ces.2006.09.003
[11] Turkyilmazoglu, M. (2011). Effects of partial slip on the analytic heat and mass transfer for the incompressible viscous fluid of a porous rotating disk flow. J Heat Transf., 133(12): 122602. https://doi.org/10.1115/1.4004558
[12] Fang, T., Zhang, J.S., Yao, J.S. (2009). Slip MHD viscous flow over a stretching sheet-an exact solution. Communications in Nonlinear Science and Numerical Simulation, 4(11): 3731-3737. https://doi.org/10.1016/j.cnsns.2009.02.012
[13] Aziz, A. (2010). Hydrodynamic and thermal slip flow boundary layer over a flat plate with constant heat flux boundary condition. Communications in Nonlinear Science and Numerical Simulation, 15(3): 573-580. https://doi.org/10.1016/j.cnsns.2009.04.026
[14] Dayyan, M., Seyyedi, S.M., Domairry, G.G., Bandpy, M.G. (2013). Analytical solution of flow and heat transfer over a permeable stretching wall in a porous medium. Math Prob Eng., 2013 Article ID 682795. http://dx.doi.org/10.1155/2013/682795
[15] Hayat, T., Qasim, M., Mesloub, S. (2011). MHD flow and heat transfer over permeable stretching sheet with slip conditions. International Journal of Numerical Methods in Fluids, 66(8): 963-975. https://doi.org/10.1002/fld.2294
[16] Mahantesh, M., Vajravelu, K., Abel, M.S., Siddalingappa, M.N. (2012). Second order slip flow and heat transfer over a stretching sheet with non-linear Navier boundary condition. International Journal of Thermal Sciences, 58: 142-150. https://doi.org/10.1016/j.ijthermalsci.2012.02.019
[17] Hayat, T., Abbasi, F.M., Al-Yami, M., Monaquel, S. (2014). Slip and Joule heating effects in mixed convection peristaltic transport of nanofluid with Soret and Dufour effects. Journal of Molecular Liquids, 194: 93-99. https://doi.org/10.1016/j.molliq.2014.01.021
[18] Abbasi, F.M., Hayat, T., Ahmad, B., Chen, G.Q. (2014). Slip effects on mixed convective peristaltic transport of copper-water nanofluid in an inclined channel. PLoS ONE, 9: e105440. https://doi.org/10.1371/journal.pone.0105440
[19] Hayat, T., Hussain, Q., Javed, T. (2009). The modified decomposition method and Pad´e approximants for the MHD flow over a non-linear stretching sheet. Nonlinear Analysis: Real World Applications, 10(2): 966-973. https://doi.org/10.1016/j.nonrwa.2007.11.020
[20] Liao, S.J. (2003). Beyond perturbation: Introduction to the homotopy analysis method. Chapman & Hall/CRC Press, Boca Raton.
[21] Rashidi, M.M., Mohimanian Pour, S.A., Abbasbandy, S. (2011). Analytic approximate solutions for heat transfer of a micropolar fluid through a porous medium with radiation. Communications in Nonlinear Science and Numerical Simulation, 16(4): 1874-1889. https://doi.org/10.1016/j.cnsns.2010.08.016
[22] Mabood, F., Khan, W.A. (2016). Analytical study for unsteady nanofluid MHD Flow impinging on heated stretching sheet. Journal of Molecular Liquids, 219: 216-223. https://doi.org/10.1016/j.molliq.2016.02.071
[23] Buongiorno, J. (2006). Convective transport in nanofluids. J Heat Transf., 128(3): 240-250. https://doi.org/10.1115/1.2150834

NOMENCLATUER

D_B	Brownian diffusion coefficient
Nb	Brownian motion parameter
L	characteristic length
Da	Darcy number
a	hydromagnetic slip parameter
L_e	Lewis number
$\bar{u}_{slip}$	linear slip velocity
C_{fx}	local friction factor
Nu_x	local Nusselt number
Sh_x	local Sherwood number
M	magnetic field parameter
C_{slip}	mass slip
E_1	mass slip factor
c	mass slip parameter
K_p	permeability of the medium
R_e	Reynolds number
f_w	suction/injection parameter
T_{slip}	thermal slip
D_1	thermal slip factor
b	thermal slip parameter
N_t	thermopheresis parameter
D_T	thermophoretic diffusion
$\bar{u},\bar{v}$	velocity component
$\bar{u}_e$	velocity of the plate
N_1	velocity slip factor

Greek symbols

α	thermal diffusivity of the fluid

τ	ratio of heat capacity
ρ_f	density of the base fluid
ρ_p	density of the nano particles
μ	dynamic viscosity of the base fluid
$(\rho C_p)_f$	heat effective heat capacity of the fluid
$(\rho C_p)_p$	effective heat capacity of the nanoparticle material